JES Focus Issue on Electrocatalysis — In Honor of Radoslav Adzic

Activation of Reduced-Graphene-Oxide Supported Pt Nanoparticles by Aligning with WO_3-Nanowires toward Oxygen Reduction in Acid Medium: Diagnosis with Rotating-Ring-Disk Voltammetry and Double-Potential-Step Chronocoulometry

Iwona A. Rutkowska,[1,*] Anna Wadas,[1] Sylwia Zoladek,[1] Magdalena Skunik-Nuckowska,[1] Krzysztof Miecznikowski,[1,*] Enrico Negro,[2] Vito Di Noto,[2,*] Agnieszka Zlotorowicz,[1,2] Piotr Zelenay,[1,3,] and Pawel J. Kulesza[1,**,z]**

[1] *Faculty of Chemistry, University of Warsaw, PL-02-093 Warsaw, Poland*
[2] *Department of Industrial Engineering, Università degli Studi di Padova in Department of Chemical Sciences, 35131 Padua (PD), Italy*
[3] *Los Alamos National Laboratory, Materials Physics and Applications, Los Alamos, New Mexico 87545, USA*

The chemically-reduced graphene-oxide has been used as support to anchor catalytic Pt nanoparticles and, while subsequently modified with tungsten oxide nanowires, has produced a hybrid electrocatalytic system for electroreduction of oxygen in acid medium. Such characteristics of reduced graphene oxide as defective surface and low degree of organization of graphitic structures facilitate dispersion of platinum nanocenters. Further combination with WO_3 nanonowires is expected to increase the system's interfacial hydrophilicity and porosity. Most likely WO_3 nanostructures are attached mainly to the edges of graphene thus preventing its stacking and creating space for the flux of oxygen and the reaction products. The results of electrochemical diagnostic experiments are consistent with the view that the electrocatalytic activity of the system utilizing tungsten oxide nanowires toward the reduction of oxygen in acid medium has been enhanced even at the Pt loading as low as 30 $\mu g\ cm^{-2}$. Furthermore, the rotating ring-disk electrode voltammetry data is consistent with decreased formation of the undesirable hydrogen peroxide intermediate in the presence of WO_3. The conclusions are supported with mechanistic and kinetic studies performed with use of double-potential-step chronocoulometry as an alternative diagnostic tool to rotating ring-disk voltammetry.

 [DOI: 10.1149/2.0491815jes]

Manuscript submitted July 25, 2018; revised manuscript received October 23, 2018. Published December 1, 2018. This was Paper 1769 presented at the Seattle, Washington Meeting of the Society, May 13–17, 2018. *This paper is part of the JES Focus Issue on Electrocatalysis — In Honor of Radoslav Adzic.*

Development of catalytic systems for oxygen reduction reaction (ORR), particularly with respect to potential applications in low-temperature fuel cells,[1–13] is still one of the most important areas of electrocatalysis. Considerable research efforts have centered on the development of Pt-free or low-Pt-content catalytic systems.[14] An ultimate goal would be to replace completely Pt with non-precious metal catalysts, e.g. by considering the metal-nitrogen/carbon compounds,[15–17] metal oxide/oxysalts,[18,19] metal-organic-frameworks[20] or just bare or functionalized carbons.[21,22] Although these nonprecious metal alternatives could exhibit in principle activities comparable to, or sometimes even better than, those characteristic of Pt in alkaline electrolytes, most of them have been less promising both in terms activity and stability (relative to Pt-based systems) in acid environments. Indeed, the commercially available applications of fuel cells (e.g. in vehicles) are mostly based on proton exchange membranes because the practical utilization of alkaline membranes is rather limited.[23–25] Consequently, serious research has been focused on improving the catalytic activity of Pt-based catalysts in acid media with less Pt loading. For example, alloying Pt with transition metals has been attempted to modify electronic structure of Pt surfaces thus resulting in improved ORR activity.[26,27] In other words, there is a need of better utilization of catalytic sites and significant lowering of the noble metal loadings.

In addition to large electrochemically active surface area and the presence of highly dispersed active sites, while exhibiting long-term stability, a useful support should prevent agglomeration of catalytic centers, facilitate oxygen mass transfer and water removal, and assure good electrical conductivity at the electrocatalytic interface. Because of the high specific surface area and excellent thermal, mechanical and electrical properties, graphene-based electrocatalysts have recently been considered. Obviously, special attention has been first devoted to noble-metal-free carbon-based (e.g. heteroatom-doped, iron or cobalt modified, totally-metal-free, functionalized or derivatized) nanomaterials including graphene-type systems.[28–34] Different concepts of utilization, including nanostructuring, doping, admixing, preconditioning, modification or functionalization of various graphene-based systems for catalytic electroreduction of oxygen have been explored.[35–46]

In the present work, we consider the chemically-reduced-graphene-oxide-supported dispersed Pt nanoparticles (loading, 30 $\mu g\ cm^{-2}$) that have been intentionally modified with tungsten oxide nanowires (loading, 300 $\mu g\ cm^{-2}$) as the catalytic system for the electroreduction of oxygen in acid medium (0.5 mol dm^{-3} H_2SO_4). Reduced graphene oxides with interfacial defects, moderate hydrophilicity, low degree of organization and porosity seem to be suitable for use as supports for anchoring noble metal nanoparticles. By analogy to graphene oxide, the existence of oxygen groups in the plane of carbon atoms of reduced graphene oxide not only tends to increase the interlayer distance but also makes the layers somewhat hydrophilic. Among other important issues are such features of tungsten oxide as porosity, large population of hydroxyl groups, high Broensted acidity, as well as fast electron transfers coupled to unimpeded proton displacements. The usefulness of WO_3 nanostructures during the reduction of oxygen was demonstrated.[4] Indeed, WO_3 was found to exhibit high reactivity toward the reductive decomposition of the hydrogen peroxide intermediate. Here, we have utilized the so-called reduced graphene oxide platelets which, contrary to conventional graphene, still contains oxygen functional groups regardless of subjecting it to the chemical reduction step.[47] It is apparent from the conventional and rotating ring-disk voltammetric measurements that the system utilizing Pt nanoparticles and reduced-graphene-oxide-supports decorated with tungsten oxide nanowires behaves as the potent O_2-reduction electrocatalytic system. Finally, the utility of

*Electrochemical Society Member.
**Electrochemical Society Fellow.
[z]E-mail: pkulesza@chem.uw.edu.pl; ilinek@chem.uw.edu.pl

double-potential-step chronocoulometry as the diagnostic tool has also been demonstrated.

Experimental

Chemical reagents were analytical grade materials. Tungsten(VI) oxide nanowires and 5% Nafion-1100 solution were purchased from Aldrich. Platinum black was obtained from Alfa Aesar. Sulfuric acid was from POCh (Gliwice, Poland).

All solutions were prepared using doubly-distilled and subsequently deionized (Millipore Milli-Q) water. They were deoxygenated by bubbling with high purity nitrogen. Measurements were made at room temperature (22 ± 2°C).

All electrochemical measurements (including voltammetry and double-potential-step chronocoulometry) were performed using a CH Instruments (Austin, TX, USA) Model 760D workstation in three electrodes configuration. The glassy carbon working electrode was utilized in a form of the disk of geometric area, 0.071 cm^2. The reference electrode was the K_2SO_4-saturated Hg_2SO_4 electrode, and the carbon rod was used as the counter electrode. All potentials reported here were recalculated and, unless otherwise stated, expressed vs. Reversible Hydrogen Electrode (RHE).

The rotating ring-disk electrode (RRDE) voltammetric experiments were conducted via variable speed rotator (Pine Instruments, USA). RRDE assembly included a glassy carbon disk (diameter 5.61 mm) and a platinum ring (inner and outer diameters were 6.25 and 7.92 mm, respectively). The collection efficiency, 0.39, was determined by usual means from the ratios of ring and disk currents obtained by performing six independent RRDE measurements at the rotation rate of 1600 rpm in the deoxygenated solution of 5 mmol dm^{-3} $K_3[Fe(CN)_6]$ and 0.01 mol dm^{-3} K_2SO_4. Prior to all electrochemical experiments the working electrode was polished with aqueous alumina slurries (grain size, 0.05 μm) on a Buehler polishing cloth.

Reduced graphene oxide (rGO) was obtained in the course of the hydrazine reduction method in an analogous manner as described before.[47] In brief, 10 ml of 50% hydrazine water solution was added to 100 ml of 0.5 wt% graphene oxide (GO) water dispersion. The mixture was heated up to 100°C and kept under stirring for 2 h.[47] After reduction, the product was filtered using polyethersulfone filter of the 0.8 μm pore size. To finalize preparation of the reduced graphene oxide (rGO) suspension, 50 mg of the resulting material was subjected to ultrasonic bath in 5 cm^3 of deionized water. Modification of glassy carbon electrode was achieved by deposition of 2 μdm^3 of the above suspension on the electrode followed by drying in air. Loading of rGO was equal to 300 μg cm^{-2}.

Suspensions (inks) of platinum black nanoparticles were prepared by dispersing 2.1 mg of the Pt commercial samples through sonication for 120 min in 2.0 cm^3 of distilled water to obtain a homogenous mixture. Later, 2 μdm^3 of the ink was placed onto the film surface to yield the noble metal loading of 30 μg cm^{-2}.

WO_3 nanowires were prepared by dispersing 1.0 mg of the material in 0.1 cm^3 of deionized water using an ultrasonic bath for 1 h. Later 2.0 μdm^3 of aqueous suspension of WO_3 nanowires was used to cover catalytic films. Loading of WO_3 nanowires was equal 300 μg cm^{-2}.

To prepare a hybrid system, first rGO was dropped as ink onto the glassy carbon electrode surface, followed by introduction of Pt nanoparticles and, at the end, by covered with the ink of tungsten oxide nanowires.

As a rule, the films were over-coated and stabilized with ultrathin layers of Nafion polyelectrolyte by depositing 1 μdm^3 of the Nafion solution (prepared by introducing 5%mass of the commercial Nafion solution into ethanol at the 1 to 10 volumetric ratio).

The catalytic materials (films) were first pre-treated in the deaerated 0.5 mol dm^{-3} H_2SO_4 electrolyte by subjecting them to repetitive potential cycling (in the range from 0.04 to 1.04 V vs. RHE) at 10 mV s^{-1} for 30 min. Before the actual electrocatalytic experiments were performed, the electrodes were conditioned by potential cycling (10 full potential cycles at 10 mV s^{-1}) in the potential range from 1.04 to 0.04 V (vs. RHE) in the oxygen-saturated 0.5 mol dm^{-3} H_2SO_4.

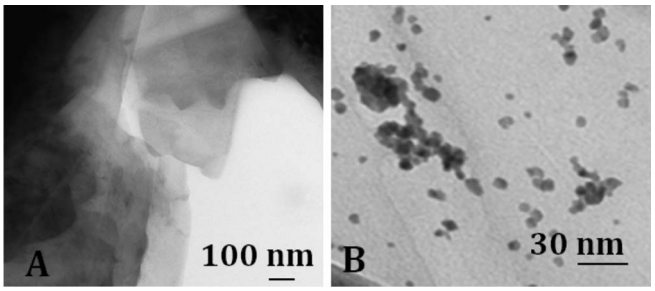

Figure 1. Transmission electron micrographs of (A) reduced graphene oxide (rGO) and (B) reduced graphene oxide supported platinum nanoparticles.

Before each representative voltammogram was recorded, the working electrode was kept for 20 s ("quiet time") at the starting potential.

Transmission electron microscopy (TEM) images were obtained with JEM 1400 (JEOL Co., Japan, 2008) equipped with high resolution digital camera (CCD MORADA, SiS-Olympus, Germany).

Results and Discussion

Physicochemical identity of graphene-supported Pt and WO_3 nanostructures.—The graphene-based catalytic materials were characterized using Transmission Electron Microscopy (TEM). It is apparent from Fig. 1 that, while the reduced graphene oxide (rGO) deposits are in a form of platelet nanostructures (Fig. 1A), the platinum nanoparticles introduced onto rGO (Fig. 1B) are largely dispersed but in some cases Pt agglomerates are formed. On mechanistic grounds, the attachment of Pt may take place at the rGO "defect" sites including surface polar groups. It is commonly accepted[36] that partially reduced graphene oxide, rGO contains various carbon–oxygen groups (hydroxyl, epoxy, carbonyl, carboxyl), in addition to the large population of water molecules still remaining in the reduced samples. Furthermore, the Raman spectra, which were reported earlier,[47] showed that intensity of the G band at 1580 cm^{-1} (reflecting graphitic structures of carbon) is rather low and the intensity the D band near 1350 cm^{-1} (originating from the amorphous structures of carbon) is relatively high. In other words, this result implies presence of interfacial defects and rather low degree of organization of the graphitic structure in the rGO material used here. Most likely WO_3 nanostructures (illustrated in Inset to Fig. 2) are attached mainly to the edges of graphene thus preventing its stacking and creating space for the flux of oxygen and the reaction products.[36]

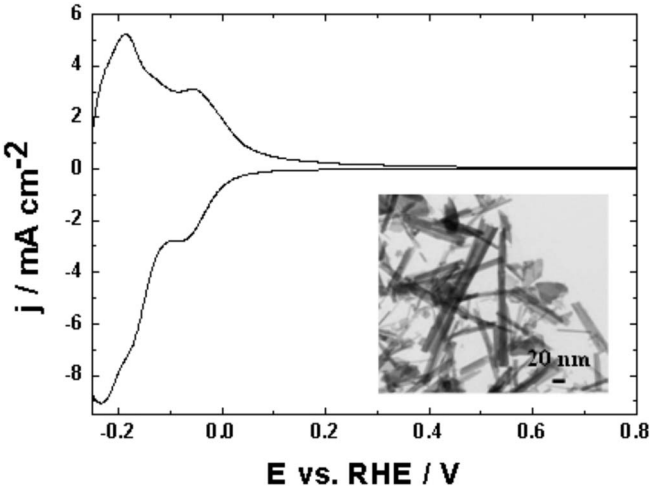

Figure 2. Cyclic voltammetry of WO_3 nanowires (deposited on the glassy carbon disk) in deoxygenated 0.5 mol dm^{-3} H_2SO_4. Scan rate, 10 mV s^{-1}. Inset illustrates transmission electron micrograph of WO_3 nanowires.

Figure 2 shows cyclic voltammetric behavior of WO_3 nanowires investigated as deposit on glassy carbon. Judging from the transmission electron micrograph of WO_3 material (Inset to Fig. 2), while diameters of the nanowires are on level of 20 nm, their lengths are in submicrometer range. Two dominanting sets of the system's voltammetric peaks appearing at potentials lower than 0.3 V reflect redox transitions of tungsten oxide consistent with the formation of two partially reduced forms of WO_3, namely hydrogen tungsten oxide bronzes of the type $H_{x1}WO_3$ and $H_{x2}WO_3$.[4] The electrochemical behavior of the latter nonstoichimetric forms is characterized by fast and reversible redox transitions. The fact, that the pair of peaks at about −0.2 V is not exactly symmetrical around the zero current axis and the reduction peak current appears relatively higher the respective oxidation one, reflects most likely contribution from the parallel irreversible generation of lower tungsten oxides, WO_{3-y}, accompanied by sorption of hydrogen.[4]

Reduction of O_2 at Pt nanoparticles deposited onto rGO-based catalysts.—The rGO-supported Pt nanoparticles are obviously less active (larger sizes and lower electrochemically active surface area) than conventional Vulcan-supported Pt during electroreduction of oxygen under conditions of the RRDE voltammetric diagnostic experiments at the comparable loadings (30 $\mu g\ cm^{-2}$). On the other hand, the rGO-supported Pt (Fig. 3A) exhibits appreciable electrocatalytic activity during reduction of oxygen in acid medium. Apparently, when acting as nanostructured support, rGO facilitates dispersion of Pt catalytic sites presumably due to its anchoring capabilities through interactions with the rGO interfacial groups. As expected from the voltammetric response recorded in the deoxygenated supporting electrolyte (dashed line in Fig. 3A), while oxidation of Pt to PtO is apparent at potentials higher than 0.7 V, the peaks existing at potentials lower than 0.35 V should attributed, as expected for Pt, to hydrogen adsorption/desorption phenomena. On the other hand, these peaks seem to be less defined and more poorly developed (in comparison to what is typically observed on clean polycrystalline platinum)[1–4] most likely due to the existence of strong interactions between immobilized Pt nanostructures and surface groups existing within rGO pores.

In the present work, we have also considered (Fig. 3B) the rGO-supported Pt nanoparticles further decorated with WO_3 nanorods (300 $\mu g\ cm^{-2}$). Comparison of the background-subtracted voltammetric responses recorded in the oxygen saturated 0.5 mol dm^{-3} H_2SO_4) shows clearly that WO_3-modified rGO-supported Pt nanoparticles exhibits relatively the highest electrocatalytic currents (curve c in Fig. 3C), relative to those recorded for the same loading of platinum deposited on the WO_3-free rGO support and the simple bare glassy carbon electrode substrate.

It is also apparent from the rotating ring-disk (RRDE) experiments (Fig. 4) that the disk (background-subtracted) currents have occurred to be higher during the reduction of oxygen at the WO_3-modified rGO-supported Pt nanoparticles (Fig. 4B) relative to the performance of pristine Pt nanoparticles deposited directly onto rGO (Fig. 4A). As expected, the ring currents which permit monitoring of the formation of the undesirable hydrogen peroxide intermediate are lower in a case of the WO_3-decorated system (Fig. 4B') relative to the performance of the bare rGO-supported Pt (Fig. 4A'). Fig. 5A illustrates the respective dependencies of limiting currents on the square root of rotation rate. The negative deviation from linearity (which is indicative of kinetic limitations) is much more pronounced for the the WO_3-free system. Also the Koutecky-Levich reciprocal plots ($I_{disk}^{-1} = (nFA\ k_s\ C_{OXYGEN})^{-1} + I_{LEVICH}^{-1}$, where k_s stands for heterogeneous rate constant and other parameters have usual significance) are characterized by higher intercepts in the latter case (Fig. 5B) thus indicating the lower k_s rate constant, $2.5*10^{-2}$ cm s^{-1}, relative to the value of $4*10^{-1}$ cm s^{-1} obtained upon addition of WO_3 nanowires. Finally, it is noteworthy that the RRDE responses summarized in Figs. 4 and 5 are characterized by reasonable stability as demonstrated by perfect reproducibility during repetitive (six independent) sets of experiments performed over the period of a week.

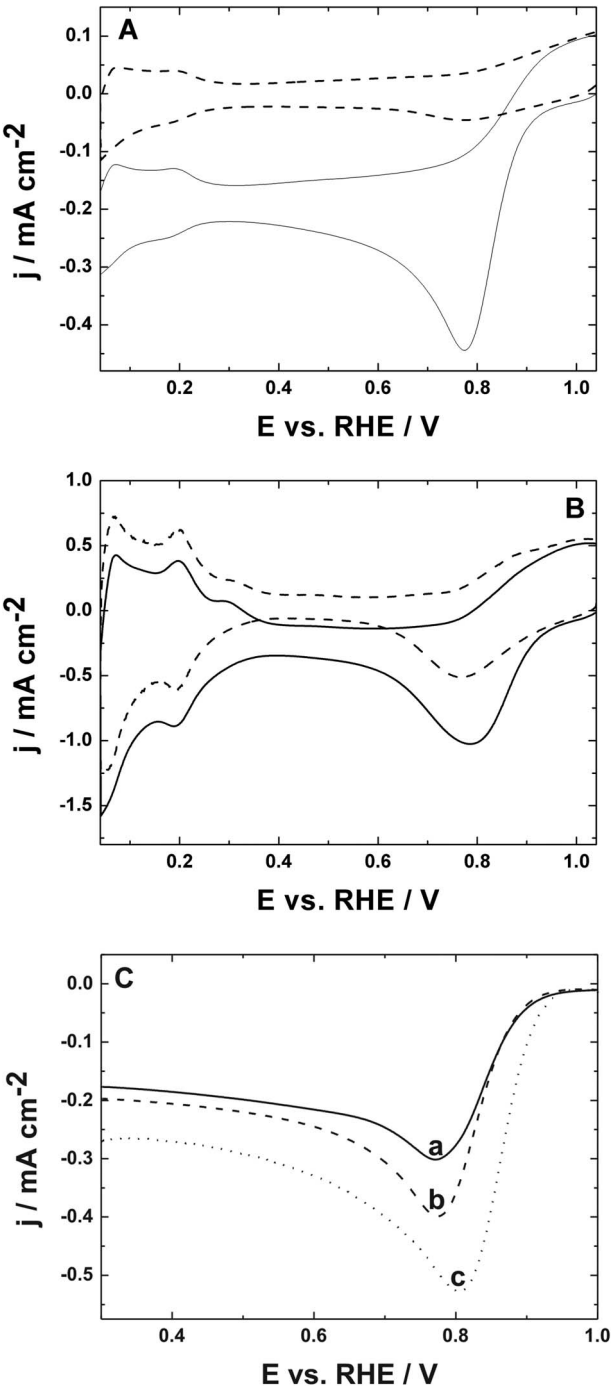

Figure 3. Voltammetric reduction of oxygen at (A) rGO-supported Pt nanoparticles and (B) rGO-supported Pt nanoparticles modified with WO_3 nanowires. (C) Background-subtracted linear scan voltammetric responses recorded for the reduction of oxygen at (a) platinum nanoparticles, (b) rGO-supported platinum nanoparticles and (c) rGO-supported platinum nanoparticles modified with WO_3 nanowires Electrolyte: oxygen-saturated 0.5 mol dm^{-3} H_2SO_4. Scan rate: 10 mV s^{-1}.

The percent amount of H_2O_2 ($\%H_2O_2$) formed during reduction of oxygen under the conditions of RRDE voltammetric experiment (e.g. at 1600 rpm rotation rate) can be estimated using the following equation:

$$\%_{H2O2} = 200^{*}I_{ring}/N/\left(I_{disk} + I_{ring}/N\right) \quad [1]$$

where I_{ring} and I_{disk} are the ring and disk currents, respectively, and N is the collection efficiency (equal to 0.39) and plotted against the

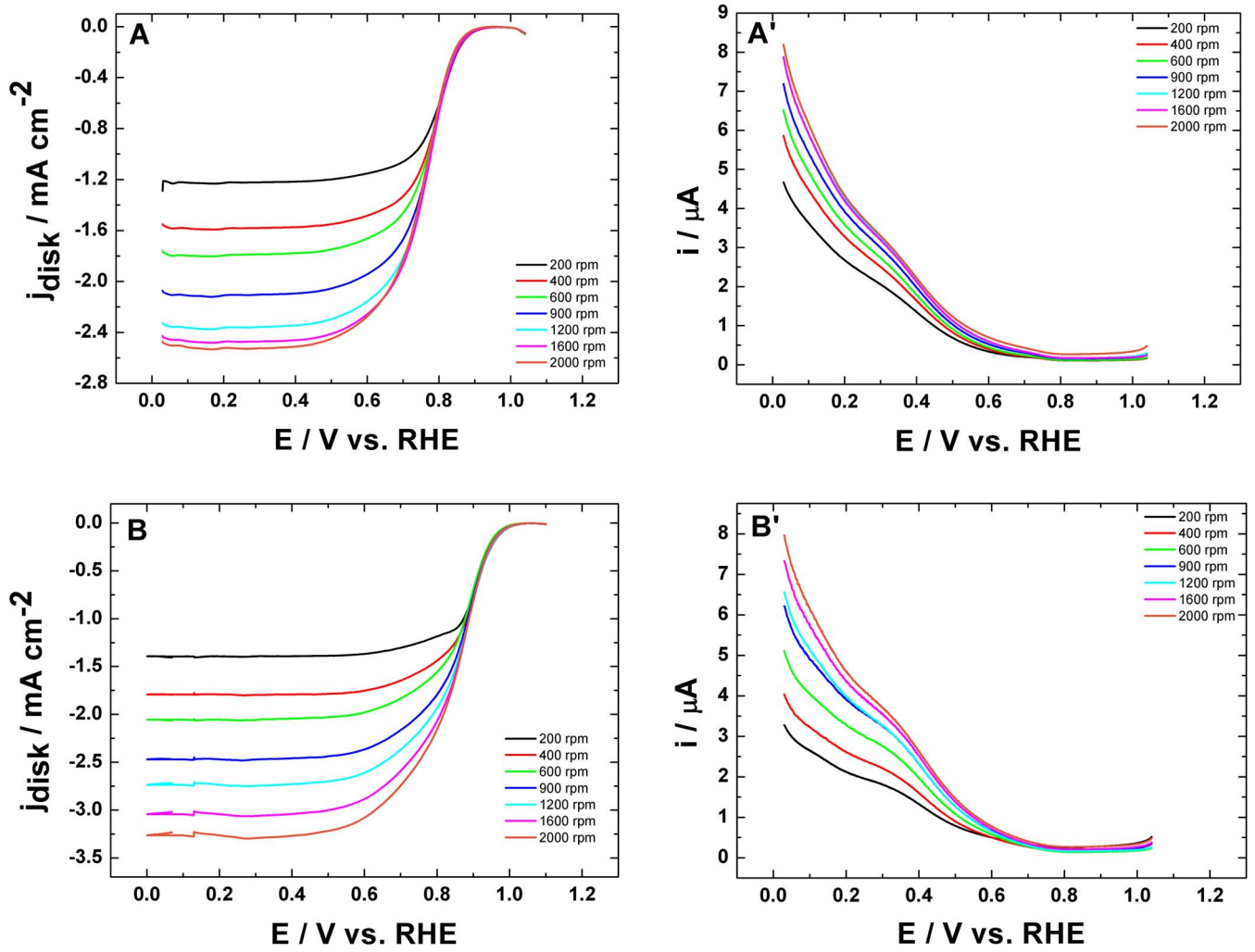

Figure 4. Normalized rotating ring-disk voltammograms for oxygen reduction at (A) rGO- supported Pt nanopartices, (B) rGO-supported Pt nanopartices modified with WO_3. Electrolyte: oxygen-saturated 0.5 mol dm^{-3} H_2SO_4. Scan rate: 10 mV s^{-1}. Ring currents are recorded upon application of 1.28 V.

applied potential (Fig. 5C). The results clearly show that the production of H_2O_2 is lower in a case of the system utilizing tungsten oxide nanowires, particularly at potentials lower than 0.4 V.

The overall number of electrons exchanged per O_2 molecule (n) can be a measure of the effectiveness of the process and has the mechanistic significance: namely it is a measure to what extent the reaction proceeds effectively according to the direct 4-electron pathway to water ($O_2 + 4H^+ + 4e- \rightarrow 2H_2O$) rather than the 2-electron one ($O_2 + 2H^+ + 2e- \rightarrow H_2O_2$) with hydrogen peroxide intermediate. Assuming that there are no other limitations, the n value was calculated and expressed as a function of the applied potential using the RRDE voltammetric data of Figs. 5A, 5A', 5B and 5B' and the equation given below:

$$n = 4^*I_{disk}/\left(I_{disk} + I_{ring}/N\right) \quad [2]$$

The corresponding number of transferred electrons (***n***) per oxygen molecule (Fig. 5D involved in the oxygen reduction was obviously higher (and closer to the ideal value of $\boldsymbol{n} = 4$) in the case of the system utilizing WO_3-decorated Pt nanoparticles supported onto rGO. The differences between the determined ***n*** values became apparent at potentials lower than 0.4 V (Fig. 5D). For example, the ***n*** values (determined at 0.1 V) were equal to 3.90 (±0.07) and 3.92 (±0.07) for the WO_3-free and WO_3-containing systems, respectively. The calculations were based on the highly reproducible (six independent) RRDE experiments at 1600 rpm; thus the standard deviations of ***n*** were on the level ±0.07.

Reduction of O_2 under chronocoulometric conditions.—An alternative and a very useful mode of recording the electrochemical responses is to integrate the current and to report charge passed as a function of time.[48,49] Chronocoulometry offers important advantages including good signal-to-noise ratio because the act of integration smooths random noise on the current transients. In comparison to chronoamperometry, by integrating the response, it is possible to separate surface phenomena (double layer-charging, surface electrochemistry) more readily from bulk electrochemical responses. When it comes to the oxygen reduction, the double-potential-step chronocoulometry permits, in principle, estimation of the number of electrons (***n***) involved in the oxygen reduction and diagnosis of formation of the hydrogen peroxide intermediate. The problem lies in understanding of the reaction kinetics and mechanisms in order to define properly experimental parameters (pulse length, starting and final potentials).

Figure 6A illustrates a representative (conventional) response for the double-potential-step experiment performed on oxygen reduction using rGO-supported Pt nanoparticles (the same catalyst as for the Fig. 5 RRDE investigations). Similar responses have been recorded for bare Pt nanoparticles as well as for the WO_3-decorated system (for simplicity not shown here). In the diagnostic experiment, the potential is shifted, or stepped, from the initial potential (e.g. 1.1 V), where insignificant electrolysis (at least in the O_2-containing H_2SO_4 solution) takes place, to the final potential of 0.3 V that is sufficiently negative to enforce a diffusion-limited current. By plotting charge (Q) versus square root of time ($t^{1/2}$), the plot of the "diffusional" charge is

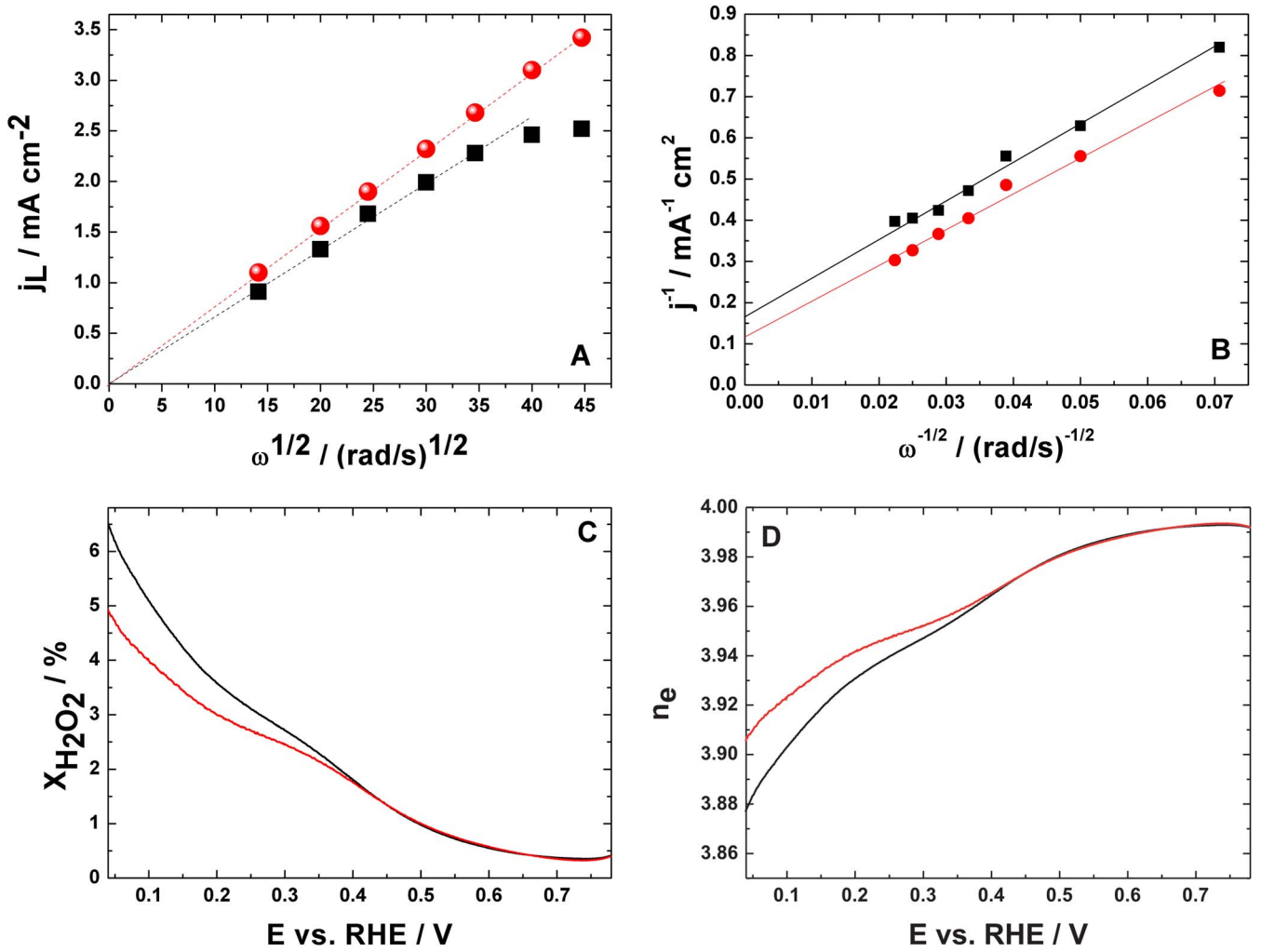

Figure 5. (A) Levich plots of current densities versus square root of rotation rate ($\omega^{1/2}$), and (B) Koutecky-Levich reciprocal plots for the electroreduction of oxygen (at 0.2 V) at rGO-supported Pt nanoparticles (black points) and rGO-supported Pt nanoparticles modified with WO_3 (red points). (C) Percent fraction of hydrogen peroxide, and (D) number of exchanged electrons during reduction of O_2 at at rGO-supported Pt nanopartices (black line), and at rGO -supported Pt nanopartices modified with WO_3 (red line).

linear (in Fig. 6B, at the $t^{1/2}$ values larger than 0.15). As expected,[48] the total charge Q vs. $t^{1/2}$ has not passed through the origin, because additional contributions to Q arising from double-layer charging and from the electroreduction of any surface species (e.g. PtO, oxygen-containing groups on rGO, etc.) including molecules (e.g. CO) that might be adsorbed at the time of application of the starting potential. The charges devoted to those processes are passed very quickly when compared to the slow accumulation of the diffusional component. Consequently, they are included in the integrated Cottrell equation by adding two time-independent terms:

$$Q = 2nF\pi^{1/2}r^2\left[D_{app}{}^{1/2}C_0\right]/t^{1/2} + Q_{dl} + nFA\Gamma_0 \qquad [3]$$

where Q_{dl} is the capacitive charge, $nFA\Gamma_0$ quantifies the faradaic component given to the reduction of the surface excess, and Γ_0 stands for surface concentration (in mol cm^{-2}), of adsorbed species. The intercept of Q vs. $t^{1/2}$ is therefore equal to $Q_{dl} + nFA\Gamma_0$. Thus chronocoulometry permits us is to comment on the surface phenomena occurring at the electrocatalytic interface as well. Simple examination of the approximate values of $nFA\Gamma_0$ (obtained by considering intercepts of the Q-$t^{1/2}$ plots in Fig. 6B and in the Inset) implies that, regardless the presence or absence of oxygen, they are comparable for both forward and reciprocal steps, respectively. In other words, the present system is well-behaved (no degradation on the time scale of the experiment) and permits pursuing further diagnostic experiments. More detailed study of the surface processes occurring at the electrocatalytic interface during reduction of oxygen will be a subject of our next communication.

The systems which can be studied using the rotating disk voltammetric methodology (including oxygen reduction) are usually well-suited for chronocoulometry because the diffusional region can be clearly established. The slopes ($Q/t^{1/2}$) of the diffusional (linear) portions of the Q vs. $t^{1/2}$ plots (Fig. 7B) can have diagnostic meaning by using the equation as follows:

$$\left[Q/t^{1/2}\right] = 2nF\pi^{1/2}r^2\left[D_{O2}{}^{1/2}C_{O2}\right] \qquad [4]$$

where r, D_{O2} and C_{O2} stand for the radius, diffusion coefficient, and concentration of redox centers (here oxygen), as well as n is a number electrons (for oxygen ideally n = 4), and F is Faraday constant (96500 C mol^{-1}). In practice, there is a need to correct the $Q/t^{1/2}$ slope determined in the presence of oxygen by subtracting the blank slope determined from the background measurement performed in the oxygen-free electrolyte (Fig. 7A).

For the oxygen saturated 0.5 mol dm^{-3} H_2SO_4 at 20°C, where $D_{O2} = 1.4{*}10^{-5}$ cm^2 s^{-1}, and $C_{O2} = 1.1{*}10^{-6}$ mol cm^{-3} (1.1 mM),[50] the theoretical value of $Q/t^{1/2}$ has been calculated to be equal to $1.18{*}10^{-4}$ C $s^{-1/2}$. Using the data, namely the background (electrolyte response) corrected slope of the liner portion of Fig. 7 (for WO_3-free rGO-supported platinum nanoparticles), the value of $Q/t^{1/2}$

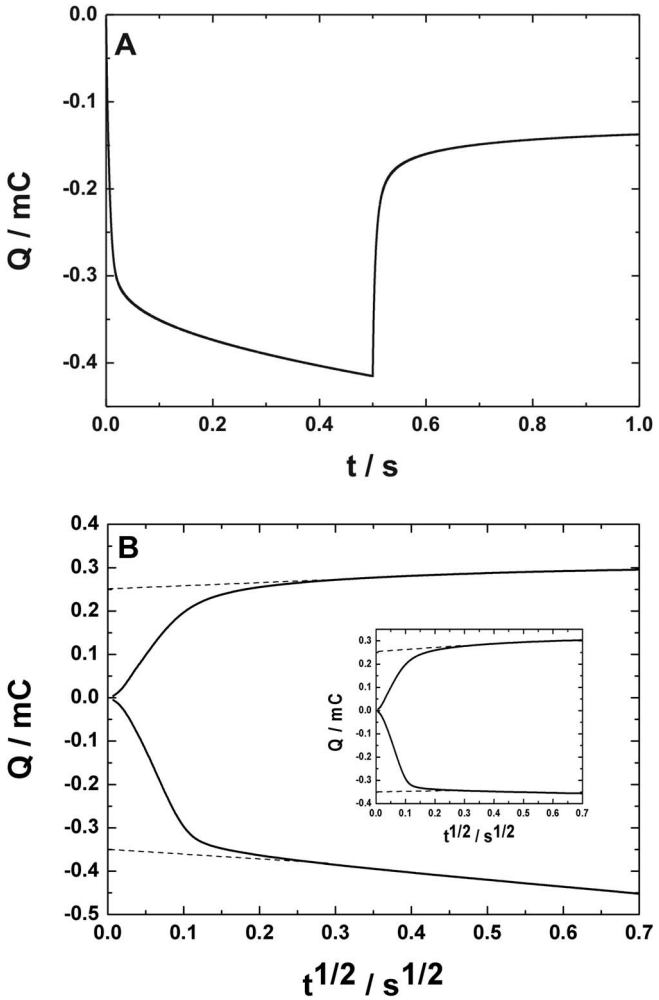

Figure 6. Double potential-step (A) chronocoulometric (conventional) and (B) chronocoulometric Anson plots responses for rGO-supported platinum nanoparticles in oxygen-saturated 0.5 mol dm^{-3} H_2SO_4. Potential steps from 1.2 to 0.3 V vs. RHE. Pulse width: 0.5 s.

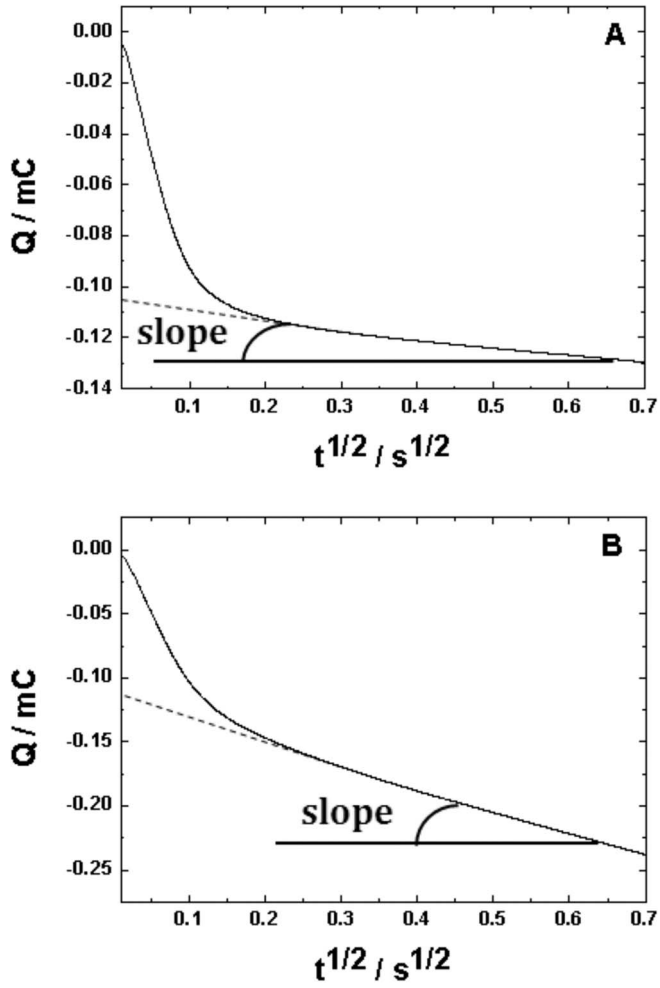

Figure 7. Chronocoulometric responses (single reduction steps) for rGO-supported platinum nanoparticles in (A) deoxygenated 0.5 mol dm^{-3} H_2SO_4, and (B) the oxygen-saturated 0.5 mol dm^{-3} H_2SO_4. Potential steps from 1.0 to 0.5 V vs. RHE. Pulse width: 0.5 s.

(slope) equal to 1.10 ($\pm$0.013)*10^{-4} C $s^{-1/2}$ has been obtained. This parameter can be determined with high accuracy (standard deviation, $\pm$0.013*10^{-4} C $s^{-1/2}$) provided that the correlation coefficient (linear fit) is on the level 0.9999. Based on Equation 4, simple comparison of the latter value to the theoretical one of 1.18 *10^{-4} C $s^{-1/2}$ implies that most likely ca. 3.7 electrons, instead of the theoretical 4 electrons, have been involved in the oxygen reduction under chronocoulometric conditions (Fig. 7) with the potential step down to 0.3 V. Using the same approach to comment on the performance of the WO_3-decorated system (graphs are for simplicity not shown here), the value of $Q/t^{1/2}$ equal to 1.14($\pm$0.014)*10^{-4} C $s^{-1/2}$ and ***n*** close to 3.9 have been determined. On the whole, these values are consistent with the RRDE results (Fig. 5D).

In the above experiments, the pulse time has been adjusted to the experimental conditions and the nature of the catalytic system just to obtain well defined linear (diffusional) portion permitting precise determination of the $Q/t^{1/2}$ slope. In general, to avoid too excessive formation of H_2O_2 intermediate, fairly short pulses (here 0.5 s) shall be used. But the potential step cannot be too short to avoid kinetic limitations and related non-linearity of the Q to $t^{1/2}$ response. In other words, the experimental conditions have to be adjusted to meet the criterion of high correlation coefficient (possibly on the level 0.9999) for the linear portion of Anson (Q to $t^{1/2}$) plot.

Application of longer pulses (e.g. 5 s) allows us to get insight into formation of the hydrogen peroxide intermediate. Under such conditions, more excessive electrolysis (oxygen reduction within the diffusional flux) is possible during the forward step thus eventually leading to some formation of H_2O_2 in the vicinity of the electrode surface. Furthermore, application of longer pulses (reduction) permits better control of background currents (it should be remembered that the responses originating from the hydrogen peroxide intermediate could be low). Immediate switching to the reverse oxidation step permits estimation of the percent of hydrogen peroxide formation. Here the maximum charges (Fig. 8) characteristic of both processes (2-electron oxidation of H_2O_2, and the approximately 4-electron reduction of O_2) should be considered. They are estimated upon assumption that diffusion coefficients of both oxygen and hydrogen peroxide are identical and by subtracting contributions originating from the material's surface processes (appearing in Fig. 8 at $t^{1/2}$ values lower than 0.2 $s^{1/2}$). It should also be remembered that different numbers of electrons are involved in both processes mentioned above. Consequently, we have found that, for the system of WO_3-free rGO-supported Pt nanoparticles, approximately 6–7% of H_2O_2 is produced. When a similar approach has been applied to the WO_3-decorated rGO-supported Pt nanoparticles (for simplicity not shown here), the amounts of hydrogen peroxide have been estimated on the level 4–5%. The approach is approximate but fast and simple. Although comparison to the RRDE data (Fig. 5C) is not straightforward because of different experimental conditions, the results of chronocoulometric estimations are consistent with our calculations based on RRDE voltammetric observations.

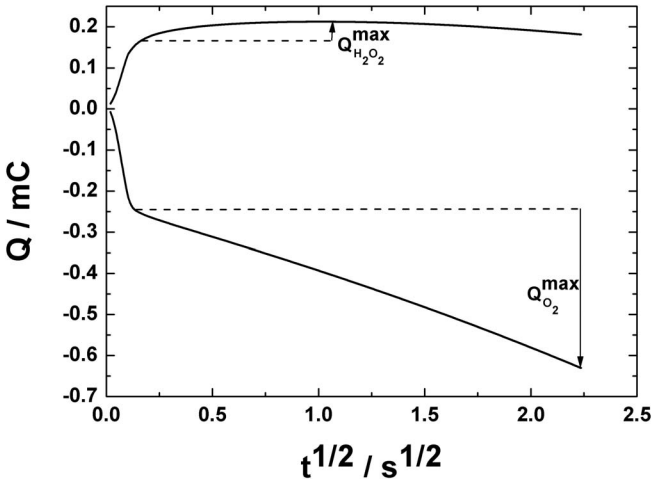

Figure 8. Background-subtracted long-pulse double-potential-step chronocoulometric (pulse width, 5s) responses recorded for rGO-supported platinum nanoparticles in oxygen-saturated 0.5 mol dm^{-3} H_2SO_4. Potential steps from 1.1 to 0.3 V vs. RHE. Here $\%H_2O_2$ has been calculated from the ratio of maximum charges for H_2O_2 oxidation ($Q_{H_2O_2}{}^{max}$) and O_2 reduction ($Q_{O2}{}^{max}$): $Q_{H_2O_2}{}^{max}/Q_{O2}{}^{max} * n_{O2}/n_{H_2O_2}$ (i.e. the ratio of the numbers of electrons involved; here approximately equal 2).

Conclusions

This study clearly demonstrates that the chemically-reduced graphene-oxide, particularly when decorated with tungsten oxide nanowires, acts as a robust and activating support for dispersed Pt nanoparticles during electrocatalytic reduction of oxygen in acid medium (0.5 mol dm^{-3} H_2SO_4). For the same low loading of catalytic Pt nanoparticles (30 $\mu g\ cm^{-2}$), decoration of the electrocatalytic interface with WO_3 results in the formation of lower amounts of the undesirable H_2O_2 intermediate. Moreover the onset potential for the oxygen reduction has been the most positive in a case of the system utilizing WO_3-decorated reduced graphene oxide. Synergistic effects and activating interactions between catalytic metal nanoparticles, tungsten oxide and nanostructured graphene supports cannot be excluded here with respect to lowering the dissociation activation energy for molecular O_2 through accelerating the charge transfer from metal in the presence of graphene and by reducing stability of the H_2O_2 intermediate species. By reviewing the RRDE parameters obtained here (such as current densities, reduction potentials, percent of the hydrogen peroxide formation) it can be stated that the electrocatalytic behavior of the WO_3-modified low-Pt-loading system is comparable, if not better, relative to the performance of other "cheap" Pt-free catalysts.[53,54]

We have also demonstrated the usefulness of the double-potential-step chronocoulometry, particularly of the charge vs. square root of time (so called Anson) plots as the fast and reliable diagnostic tool for evaluation of the effectiveness of the oxygen reduction. This work parallels other recent attempts to use chronocoulometry in the oxygen reduction research.[51,52] In the present work, we have demonstrated that, by proper adjustment of pulse times and other experimental parameters within the double-potential-step experiment, mechanistic considerations permitting estimation of the number of electrons involved and the percent of formation of the H_2O_2 intermediate are feasible.

Acknowledgments

We acknowledge the European Commission through the Graphene Flagship – Core 1 project [grant number GA-696656] and Maestro Project [2012/04/A/ST4/00287 (National Science Center, Poland)]. Many thanks for Dr. Leszek Stobinski for donating us reduced graphene oxide.

ORCID

Iwona A. Rutkowska https://orcid.org/0000-0002-8785-8733
Vito Di Noto https://orcid.org/0000-0002-8030-6979
Pawel J. Kulesza https://orcid.org/0000-0002-6150-8049

References

1. M. Shao, Q. Chang, J.-P. Dodelet, and R. Chenitz, *Chem. Rev.*, **116**, 3594 (2016).
2. Y.-J. Wang, N. Zhao, B. Fang, H. Li, X. T. Bi, and H. Wang, *Chem. Rev.*, **115**, 3433 (2015).
3. N. V. Long, Y. Yang, C. M. Thi, N. Van Minh, Y. Cao, and M. Nogami, *Nano Energy*, **2**, 636 (2013).
4. A. Lewera, K. Miecznikowski, R. Hunger, A. Kolary-Zurowska, A. Wieckowski, and P. J. Kulesza, *Electrochim. Acta*, **55**, 7603 (2010).
5. I. Katsounaros, S. Cherevko, A. R. Zeradjanin, and K. J. J. Mayrhofer, *Angew. Chem. Int. Ed.*, **53**, 102 (2014).
6. R. Bashyam and P. Zelenay, *Nature*, **443**, 63 (2006).
7. J. Masa, A. Zhao, W. Xia, M. Muhler, and W. Schuhmann, *Electrochim. Acta*, **128**, 271 (2014).
8. M. A. Hickner, A. M. Herring, and E. B. Coughlin, *J. Polym. Sci. Part B Polym. Phys.*, **51**, 1727 (2013).
9. N. Ramaswamy and S. Mukerjee, *J. Phys. Chem. C*, **115**, 18015 (2011).
10. L. Qu, Y. Liu, J. B. Baek, and L. Dai, *ACS Nano*., **4**, 1321 (2010).
11. B. C. Steele and A. Heinzel, *Nature*, **414**, 345 (2001).
12. Y. Nie, L. Li, and Z. Wei, *Chem. Soc. Rev.*, **44**, 2168 (2015).
13. D. Schonvogel, J. Hulstede, P. Wagner, I. Kruusenberg, K. Tammeveski, A. Dyck, C. Agert, and M. Wark, *J. Electrochem. Soc.*, **164**, F995 (2017).
14. A. Morozan, B. Jousselme, and S. Palacin, *Energy Environ. Sci.*, **4**, 1238 (2011).
15. U. I. Kramm, I. Herrmann-Geppert, J. Behrends, K. Lips, S. Fiechter, and P. Bogdanoff, *J. Am. Chem. Soc.*, **138**, 635 (2016).
16. Y. Hu, J. O. Jensen, W. Zhang, L. N. Cleemann, W. Xing, N. J. Bjerrum, and Q. Li, *Angew. Chem. Int. Ed.*, **53**, 3675 (2014).
17. J. Zhang, Q. Li, H. Wu, C. Zhang, K. Cheng, H. Zhou, M. Pan, and S. Mu, *J. Mater. Chem. A*, **3**, 10851 (2015).
18. Y. Liang, Y. Li, H. Wang, J. Zhou, J. Wang, T. Regier, and H. Dai, *Nat. Mater.*, **10**, 780 (2011).
19. T. Zhou, Y. Du, S. Yin, X. Tian, H. Yang, X. Wang, B. Liu, H. Zheng, S. Qiao, and R. Xu, *Energy Environ. Sci.*, **9**, 2563 (2016).
20. M. Jahan, Z. Liu, and K. P. Loh, *Adv. Funct. Mater.*, **23**, 5363 (2013).
21. I. A. Khan, Y. Qian, A. Badshah, M. A. Nadeem, and D. Zhao, *ACS Appl. Mater. Interfaces*, **8**, 17268 (2016).
22. L. Cao, Z. Lin, J. Huang, X. Yu, X. Wu, B. Zhang, Y. Zhan, F. Xie, W. Zhang, J. Chen, W. Xie, W. Mai, and H. Meng, *Int. J. Hydrogen Energy*, **42**, 876 (2017).
23. J. Pan, S. Lu, Y. Li, A. Huang, L. Zhuang, and J. Lu, *Adv. Funct. Mater.*, **20**, 312 (2010).
24. J. R. Varcoe, P. Atanassov, D. R. Dekel, A. M. Herring, M. A. Hickner, P. A. Kohl, A. R. Kucernak, W. E. Mustain, K. Nijmeijer, K. Scott, T. Xu, and L. Zhuang, *Energy Environ. Sci.*, **7**, 3135 (2014).
25. J. R. Varcoe, R. C. T. Slade, and E. L. H. Yee, *Chem. Commun.*, **3**, 1428 (2006).
26. C. Wang, M. Chi, D. Li, D. Strmcnik, D. van der Vliet, G. Wang, V. Komanicky, K. C. Chang, A. P. Paulikas, D. Tripkovic, J. Pearson, K. L. More, N. M. Markovic, and V. R. Stamenkovic, *J. Am. Chem. Soc.*, **133**, 14396 (2011).
27. D. He, L. Zhang, D. He, G. Zhou, Y. Lin, Z. Deng, X. Hong, Y. Wu, C. Chen, and Y. Li, *Nat. Commun.*, **7**, 12362 (2016).
28. S. Zoladek, I. A. Rutkowska, M. Blicharska, K. Miecznikowski, W. Ozimek, J. Orlowska, E. Negro, V. Di Noto, and P. J. Kulesza, *Electrochim. Acta*, **233**, 113 (2017).
29. J.-C. Li, P.-X. Hou, and C. Liu, *Small*, 1702002 (2017).
30. D. K. Perivoliotis and N. Tagmatarchis, *Carbon*, **118**, 493 (2017).
31. G. Fazio, L. Ferrighi, D. Perilli, and C. Di Valentin, *Int. J. Quantum. Chem.*, **116**, 1623 (2016).
32. C. R. Raj, A. Samanta, S. H. Noh, S. Mondal, T. Okajima, and T. Ohsaka, *J. Mater. Chem. A*, **4**, 11156 (2016).
33. D. Higgins, P. Zamani, A. Yu, and Z. Chen, *Energy Environ. Sci.*, **9**, 357 (2016).
34. X. Huang, X. Qi, F. Boey, and H. Zhang, *Chem. Soc. Rev.*, **41**, 666 (2012).
35. E. Quesnel, F. Roux, F. Emieux, P. Faucherand, E. Kymakis, G. Volonakis, F. Giustino, B. Martín-García, I. Moreels, S. A. Gürsel, A. B. Yurtcan, V. Di Noto, A. Talyzin, I. Baburin, D. Tranca, G. Seifert, L. Crema, G. Speranza, V. Tozzini, P. Bondavalli, G. Pognon, C. Botas, D. Carriazo, G. Singh, T. Rojo, G. Kim, W. Yu, C. P. Grey, and V. Pellegrini, *2D Mater.*, **2**, 030204 (2015).
36. P. J. Kulesza, J. K. Zak, I. A. Rutkowska, B. Dembinska, S. Zoladek, K. Miecznikowski, E. Negro, V. Di Noto, and P. Zelenay, *Curr. Opin. Electrochem.*, **9**, 257 (2018).
37. C. Zhu and S. Dong, *Nanoscale*, **5**, 1753 (2013).
38. K. Parvez, S. Yang, Y. Hernandez, A. Turchanin, X. Feng, and K. Mullen, *ACS Nano*, **6**, 9541 (2012).
39. Y. Liang, Y. Li, H. Wang, and H. Dai, *J. Am. Chem. Soc.*, **135**, 2013 (2013).
40. T. Li, Q. Wang, S. Dou, Z. Ma, J. Huo, S. Wang, and L. Dai, *Chem. Comm.*, **52**, 2764 (2016).
41. B. Seger and P. V. Kamat, *J. Phys. Chem. C*, **113**, 7990 (2009).
42. X. Zhong, Y. Qin, X. Chen, W. Xu, G. Zhuang, X. Li, and J. Wang, *Carbon*, **114**, 740 (2017).

43. P. J. Kulesza, B. Dembinska, S. Zoladek, I. A. Rutkowska, K. Miecznikowski, E. Negro, and V. Di Noto, *ECS Trans.*, **80**, 869 (2017).
44. G. Zhang, W. Lu, F. Cao, Z. Xiao, and X. Zheng, *J. Power Sources*, **302**, 114 (2016).
45. E. Negro, A. B. Delpeuch, K. Vezzù, G. Nawn, F. Bertasi, A. Ansaldo, V. Pellegrini, B. Dembinska, S. Zoladek, K. Miecznikowski, I. A. Rutkowska, M. Skunik-Nuckowska, P. J. Kulesza, F. Bonaccorso, and V. Di Noto, *Chem. Matter.*, **30**, 2651 (2018).
46. Y. Shao, S. Zhang, C. Wang, Z. Nie, J. Liu, Y. Wang, and Y. Lin, *J. Power Sources*, **195**, 4600 (2010).
47. L. Stobinski, B. Lesiak, A. Malolepszy, M. Mazurkiewicz, B. Mierzwa, J. Zemek, P. Jiricek, and I. Bieloshapka, *J. Electron. Spectrosc. Relat. Phenom.*, **195**, 145 (2014).
48. A. J. Bard and L. R. Faulkner, in *Electrochemical Methods*, VCH, New York, 1994.
49. F. C. Anson, *Anal. Chem.*, **38**, 54 (1966).
50. C. Song and J. Zhang, in *PEM Fuel Cell Electrocatalysts and Catalyst Layers. Fundamentals and Applications*, J. Zhang Editor, p. 89, Springer-Verlag London (2008).
51. L. Xu, G. Zhang, J. Chen, Y. Zhou, G. Yuan, and F. Yang, *J. Power Source*, **240**, 101 (2013).
52. I. Kocak, *Anal. Lett.*, **50**, 1448 (2017).
53. H. T. Chung, G. Wu, Q. Li, and P. Zelenay, *Int. J. Hydrogen Energy*, **39**, 15887 (2014).
54. Q. Jia, N. Ramaswamy, H. Hafiz, U. Tylus, K. Strickland, G. Wu, B. Barbiellini, A. Bansil, E. F. Holby, P. Zelenay, and S. Mukerjee, *ACS Nano*, **9**, 12496 (2015).